NANO LETTERS

pubs.acs.org/NanoLett Letter

Enhanced H_2O_2 Upcycling into Hydroxyl Radicals with GO/Ni:FeOOH-Coated Silicon Nanowire Photocatalysts for Wastewater Treatment

Rui Ning, Sungsoon Kim, Eddie Sun, Yue Jiang, Jihyun Baek, Yuzhe Li, Ashley Robinson, Lauren Vallez, and Xiaolin Zheng*

Cite This: *Nano Lett.* 2023, 23, 6323−6329 Read Online

ABSTRACT: There remains continued interest in improving the advanced water oxidation process [e.g., ultraviolet (UV)/hydrogen peroxide (H_2O_2)] for more eficient and environmentally friendly wastewater treatment. Here, we report the design, fabrication, and performance of graphene oxide (GO, on top)/nickel-doped iron oxyhydroxide (Ni:FeOOH, shell)/silicon nanowires (SiNWs, core) as a new multifunctional photocatalyst for the degradation of common pollutants like polystyrene and methylene blue through enhancing the hydroxyl radical (•OH) production rate of the UV/H_2O_2 system. The photocatalyst combines the advantages of a large surface area and light absorption characteristics of SiNWs with heterogeneous photo-Fenton active Ni:FeOOH and photocatalytically active/charge separator GO. In addition, the built-in electric field of GO/Ni:FeOOH/SiNWs facilitates the charge separation of electrons to GO and holes to Ni:FeOOH, thus boosting the photocatalytic performance. Our photocatalyst increases the •OH yield by 5.7 times compared with that of a blank H_2O_2 solution sample and also extends the light absorption spectrum to include visible light irradiation.

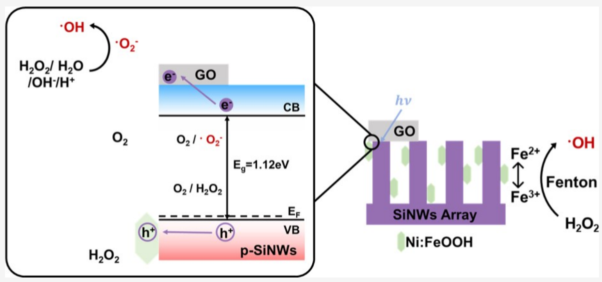

KEYWORDS: *silicon nanowires, hydroxyl (OH) radicals, wastewater treatment, photocatalysis, photo-Fenton reaction*

On-demand, local, small-scale, affordable, and effective purification of various types of water sources is vitally important for water sustainability and security, especially in underdeveloped areas of the world. Advanced oxidation processes (AOPs) are a class of effective methods for water purification that combine a green oxidizer such as H_2O_2 with ultraviolet (UV) irradiation, ozone, or ferrous ions (Fe^{2+}, typically from $FeSO_4$) to produce highly reactive •OH. As a powerful oxidizing agent, •OH is an effective disinfectant for the removal of many microorganisms and organic contaminants.[1−5] Among AOPs, the combination of H_2O_2 with UV (UV/H_2O_2) destroys harmful microorganisms during wastewater treatment and does not produce potentially harmful ions as byproducts like in UV/peroxydisulfate- and UV/H_2O_2/$NaHCO_3$-based processes.[6] However, the UV/H_2O_2 process is inherently limited as H_2O_2 itself has poor UV absorption properties[7] that cannot be simply addressed by increasing the H_2O_2 concentration as excess H_2O_2 can recombine with •OH to form water.[7]

One approach for enhancing the •OH production rate of the UV/H_2O_2 process is to include the Fenton process (eqs R1 and R2) as a reaction pathway,[8−10] i.e., the photo-Fenton (UV/H_2O_2/Fe^{2+}) process. However, the Fenton reaction is not easily reversible, as the oxidation of Fe^{2+} to Fe^{3+} (eq R1) is much faster than the regeneration of Fe^{2+} through the reaction between Fe^{3+} and H_2O_2 (eq R2), leading to the formation of ferric sludge. This can be partially mitigated by the inclusion of UV irradiation, which accelerates the conversion of Fe^{3+} to Fe^{2+} (eqs R3 and R4), thereby enhancing the •OH production rate.[8] In addition, the eficiency of the photo-Fenton process can be further improved by increasing the catalyst surface area, enhancing light absorbance, and improving charge transfer.[8]

$$Fe^{2+} + H_2O_2 \rightarrow Fe^{3+} + \bullet OH + OH^- \quad (R1)$$

$$Fe^{3+} + H_2O_2 \rightarrow Fe^{2+} + \bullet HO_2 + H^+ \quad (R2)$$

$$Fe^{3+} + h\nu + H_2O_2 \rightarrow Fe^{2+} + \bullet HO_2 + H^+ \quad (R3)$$

$$Fe^{3+} + h\nu + H_2O \rightarrow Fe^{2+} + \bullet OH + H^+ \quad (R4)$$

Traditional Fenton reactions use Fe salts as a homogeneous catalyst, but this limits the process operation window to ≈3 pH

Received: February 21, 2023
Revised: July 9, 2023
Published: July 17, 2023

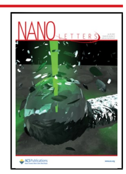

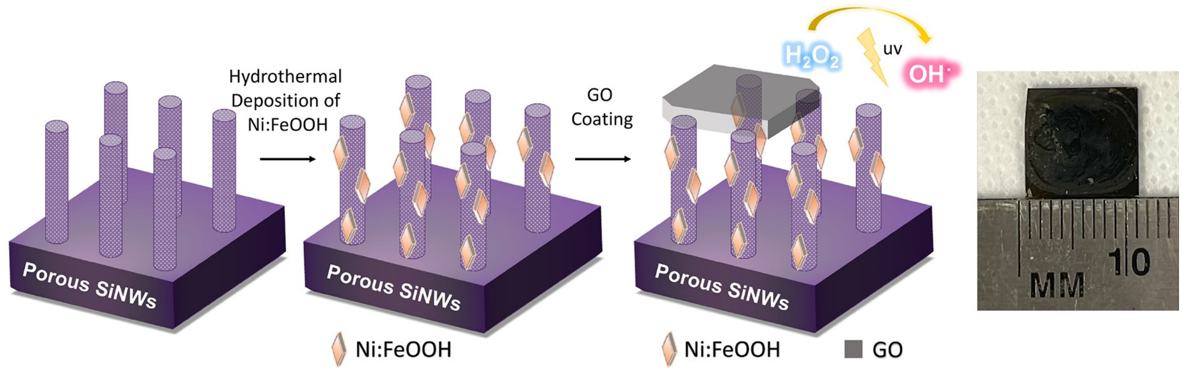

Figure 1. Process flow schematic of the procedure for the synthesis of GO/Ni:FeOOH/SiNWs and a photograph of the fabricated sample (1 cm × 1 cm).

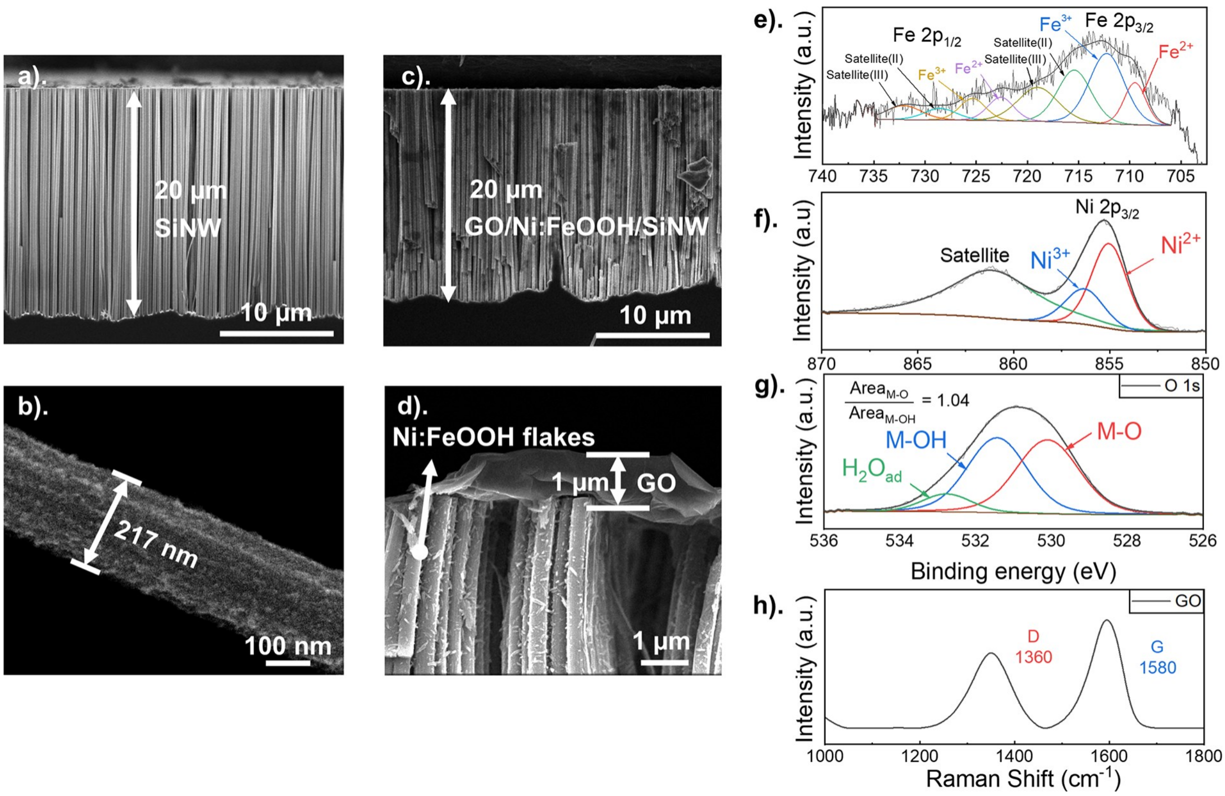

Figure 2. SEM side view images of the SiNWs (a) before and (c) after GO/Ni:FeOOH coating. (b) SEM image of a single porous SiNW. (d) SEM image of the GO/Ni:FeOOH/SiNWs. XPS spectra of (e) Fe 2p, (f) Ni 2p, and (g) O 1s in GO/Ni:FeOOH/SiNWs.[26−28] Ni^{2+} and Fe^{3+} are the majority species. (h) Raman spectra of the GO/Ni:FeOOH/SiNWs.

and has inherent challenges related to the separation and reuse of catalysts. Accordingly, considerable efforts have been devoted to the design of heterogeneous Fe-based catalysts for the heterogeneous Fenton reaction,[11] which allow for considerably easier downstream separation. For example, iron(III) oxyhydroxide (FeOOH), a stable and environmentally friendly natural mineral, has been found to be an effective catalyst for the heterogeneous photo-Fenton process.[12,13] Studies have shown that the catalytic efficiency of FeOOH can be improved by Ni doping, which mitigates the problem of Fe^0 passivation and agglomeration for the removal of organic pollutants.[14,15]

The choice of a photoabsorber when utilizing UV irradiation to enhance the •OH production rate is also important. Silicon is a logical first choice as it is abundant and environmentally friendly with great light absorption properties, as it is used in solar cell[16,17] and photodetector[18] applications. In particular, the light-trapping effects and large specific surface areas of silicon nanowires (SiNWs) are highly desired for photocatalysis applications and SiNWs have been previously shown to produce radical and reactive oxygen species (ROS) for photochemistry.[19,20] Moreover, a graphene oxide (GO) top coating was found to considerably increase the photocatalytic activity of the array of SiNWs.[21,22] Since all of these strategies separately have been shown to increase photocatalytic productivity, it is logical to combine the benefits of SiNWs, Ni-doped FeOOH (Ni:FeOOH), and GO for the photo-Fenton process to increase the rate of production of •OH.

In this work, we report on the design, fabrication, and photocatalytic performance of a new multifunctional photo-

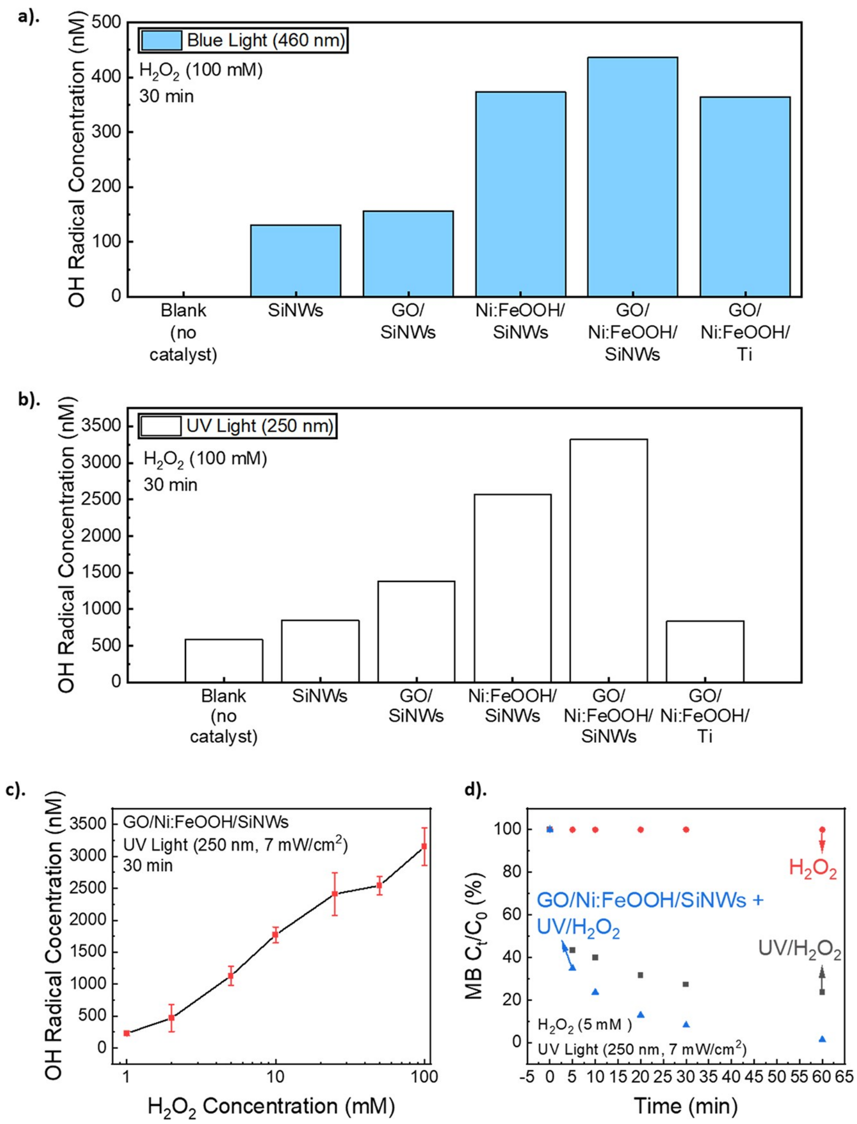

Figure 3. •OH concentrations of blank H_2O_2, bare SiNWs, GO/SiNWs, Ni:FeOOH/SiNWs, GO/Ni:FeOOH/SiNWs, and GO/Ni:FeOOH/Ti under (a) blue light (460 nm) and (b) UV light (250 nm) irradiation with 100 mM H_2O_2 for 30 min (samples without H_2O_2 have no •OH generation). (c) •OH generation vs H_2O_2 concentration for GO/Ni:FeOOH/SiNWs with the standard deviation error bars from six measurements at each condition. (d) Time-dependent 50 μM MB degradation plot of GO/Ni:FeOOH/SiNWs in 5 mM H_2O_2 solutions under 7 mW/cm^2 250 nm UV light for 60 min (all samples have no •OH generation at time zero).

catalyst, GO/Ni:FeOOH/SiNWs, which contains Ni:FeOOH (shell)/SiNW (core) core/shell nanowires with GO flakes coated on top of the nanowire arrays to enhance the rate of production of •OH for the UV/H_2O_2 system. The GO/Ni:FeOOH/SiNW photocatalyst combines the advantages of a large surface area and light absorption characteristics of SiNWs with heterogeneous photo-Fenton active Ni:FeOOH and charge carrier separator GO.[21,23] The use of this photocatalyst increases the •OH yield by 5.7 times compared to that of the blank H_2O_2 solution sample and also extends the irradiation absorption spectrum to include UV and visible light. Quantitatively, the produced •OH concentration reaches 3.32 μM (0.332%) from 100 mM H_2O_2 after 250 nm (7 mW/cm2) UV light irradiation for 30 min. We demonstrate that the GO/Ni:FeOOH/SiNW photocatalyst is capable of degrading 50 μM MB to 1.5% of its original concentration after 250 nm UV irradiation for 60 min in 5 mM H_2O_2 and is capable of decreasing the diameter of 500 nm PS particles to ∼400 nm after UV irradiation for 24 h in 100 mM H_2O_2. Overall, these results demonstrate that the production of •OH from the UV/H_2O_2 system can be greatly enhanced by the multifunctional GO/Ni:FeOOH/SiNW photocatalyst, which also demonstrates its potential eficacy for wastewater treatment and plastic degradation.

Figure 1 illustrates the process for the fabrication of GO/Ni:FeOOH/SiNWs. It starts with the synthesis of porous SiNWs by metal-assisted anodic etching (MAAE), followed by surface coating of Ni:FeOOH by hydrothermal deposition and top coating of GO by drop casting. Specifically, the porous SiNWs (∼20 μm) were prepared from Si wafers (p-type, boron-doped, 1000 μm, 0.001−0.005 Ω cm) by MAAE as described in our previous work[24,25] with 4.8 M hydrofluoric acid (HF). Next, the surface of porous SiNWs was coated with Ni:FeOOH flakes by the hydrothermal deposition method.[15] Briefly, two separate solutions of 30 mM $FeCl_3$ and 30 mM $NiCl_2$ in deionized (DI) water were prepared. In both solutions, 45 mM urea was added to serve as the progressive OH^--releasing agent. Next, the $FeCl_3$ and $NiCl_2$ solutions were mixed in a volumetric ratio of 1:700 to prepare a 25 mL precursor solution. The SiNW pieces (1 cm × 1 cm) were placed sideways in the precursor solution container, and the sample was held at 100 °C for 45 min in an oven. Then, the Ni:FeOOH-coated SiNWs were washed with DI water and dried with an air gun. Finally, the Ni:FeOOH-coated SiNWs were further coated with GO (purchased from Graphenea) by dropping ∼1 mL of GO in a DI water solution (1 mg/50 mL) three times before drying at 50 °C on a hot plate. The Supporting Information contains further details about the characterization and testing of the materials.

Porous SiNWs in GO/Ni:FeOOH/SiNWs fabricated as described in Figure 1 are in the form of vertical arrays that are ∼20 μm in length (Figure 2a) and ∼200 nm in diameter (Figure 2b). The 20 μm length of SiNW was chosen because such a SiNW length has been previously shown to be suficiently long to absorb the majority of the UV light.[21] Additionally, the 500 and 20 μm long SiNWs generate approximately the same amount of •OH in our system (Figure S3), thereby demonstrating that the 20 μm SiNW is suficiently thick for maximum •OH generation.

The Ni:FeOOH flakes were uniformly coated along the length of the SiNWs, while the GO layers were coated on top of the SiNWs with a thickness of ∼1 μm (Figure 2d). The SiNW morphology appears to remain constant after Ni:FeOOH and GO coating (Figure 2c). Fe 2p X-ray photoelectron spectroscopy (XPS) spectra consist of four distinguishable peaks of Fe $2p_{3/2}$, Fe $2p_{1/2}$, and their satellite peaks (Figure 2e). The deconvolved Fe 2p XPS spectra showed a mixed state of Fe^{2+} and Fe^{3+} in both Fe $2p_{3/2}$ and Fe $2p_{1/2}$ with the Fe^{3+} state as the major oxidation state (indicative of FeOOH). Meanwhile, Ni 2p XPS spectra were deconvolved into three distinct peaks of Ni^{2+}, Ni^{3+}, and satellite peaks (Figure 2f), with Ni^{2+} being the dominant phase. The O 1s XPS spectrum (Figure 2g) was deconvolved into three different peaks, where M−O, M−OH, and adsorbed H_2O on the Ni:FeOOH surface were located at 530.1, 531.4, and 532.8 eV, respectively.[29] Because the crystal structure of FeOOH is composed of an equal amount of M−O and M−OH and the area ratio of deconvoluted M−O and M−OH peaks is 1.04, this confirms the presence of FeOOH.

XPS and X-ray diffraction (XRD) spectra were compared before and after •OH generation experiments (∼5 h) in a H_2O_2 solution to evaluate the catalyst stability. The XPS spectra of the GO/Ni:FeOOH/SiNWs samples were also deconvolved into their characteristic peaks and no obvious changes in their XPS spectra were observed (Figure S4a−c). Some Si in the SiNWs was converted into SiO_2 by oxidation during the photocatalytic reaction as evidenced when comparing the Si XRD peak at 28.4° and the SiO_2 XRD peak at 32.9° (Figure S5). This phenomenon is expected as the surface of Si is spontaneously oxidized in water, but the majority of the Si phase remains even after a photocatalytic reaction for a few hours (Figure S5). Therefore, the SiNW is relatively stable and reusable after the photocatalytic reaction. However, the concentration of Ni:FeOOH in GO/Ni:FeOOH/SiNWs is low so it cannot be detected or analyzed in the XRD spectra before or after the •OH generation experiments. Collectively, the XPS, Raman, and XRD results strongly suggest that the samples of GO/Ni:FeOOH/SiNWs are relatively stable even after long reaction times (∼5 h).

The scanning electron microscopy-energy dispersive X-ray spectroscopy (SEM-EDS) results in Figure S6 confirm the existence of Fe and O in the region of SiNWs. The Raman spectra of GO in Figure 2h and Figure S4c show the characteristic D band and G band peaks before and after the •OH generation experiments, confirming the existence of carbon in the samples of GO/Ni:FeOOH/SiNWs. These results collectively also confirm the presence of all individual components of GO/Ni:FeOOH/SiNWs.

First, we compared the amount of •OH generated from H_2O_2 using five photocatalysts: blank (no catalyst), SiNWs, GO/SiNWs, Ni:FeOOH/SiNWs, GO/Ni:FeOOH/SiNWs, and GO/Ni:FeOOH/Ti. Panels a and b of Figure 3 plot the measured •OH concentration after blue and UV light irradiation for 30 min. UV irradiation produces more •OH than blue light for all of the photocatalysts. We note that the introduction of the photocatalysts enables •OH production with blue light; no •OH production was observed with blue light irradiation without a photocatalyst present (Figure 3a). The amount of •OH produced depends strongly on the photocatalyst. Under the same irradiation conditions, the •OH concentration increases in the following order: SiNWs < GO/SiNWs < Ni:FeOOH/SiNWs < GO/Ni:FeOOH/SiNWs. The amount of •OH generated by GO/Ni:FeOOH/SiNWs is ∼4 times that of SiNWs and 2 times that of GO/SiNWs under UV irradiation. This difference cannot be explained by the light absorption difference alone as the coating of Ni:FeOOH and GO/Ni:FeOOH increases the average light absorption of SiNWs (∼79%) at 460 nm by only ∼3.7% and ∼6.8% (Figure S7), respectively. Note that SiNW is the major light absorber, which accordingly generates e^- and h^+ pairs to produce radicals, while the Fe species in Ni:FeOOH is the active photo-Fenton reaction catalyst that can produce additional radicals.

SiNWs are a semiconductor material in which the band structure affects charge carrier harvesting. Thus, to confirm the contribution of GO and Ni:FeOOH to the improved •OH generation performance of GO/Ni:FeOOH/SiNWs, we prepared GO/Ni:FeOOH on a Ti mesh (without SiNW) and compared their photocatalytic performance. •OH generation was still observed on GO/Ni:FeOOH/Ti under both blue light and UV light irradiation (Figure 3a,b), due to the photo-Fenton reaction in our system. Interestingly, the •OH concentration of GO/Ni:FeOOH/SiNW observed after UV light irradiation is higher than the sum of the OH concentrations of SiNW and GO/Ni:FeOOH samples, which indicates that the heterojunction effect that modulates the Si band structure is more favorable to charge carrier harvesting in GO/Ni:FeOOH/SiNWs.

Next, we studied the effect of the H_2O_2 concentration on •OH generation. We used the best-performing GO/Ni:FeOOH/SiNWs as the photocatalyst and measured the •OH concentration after UV irradation (250 nm, 7 mW/cm^2) for 30 min at different initial H_2O_2 concentrations. The exponential increase in the H_2O_2 concentrations results in only a linear increase in the generated •OH concentration as shown in the semilog plot in Figure 3c. This result suggests that increasing the concentration of H_2O_2 has a limited, non-proportional impact on promoting •OH generation, which is supported by previous observations reported in the literature that a higher concentration of H_2O_2 is detrimental to •OH generation due to the scavenging effect of •OH (•OH + H_2O_2 → •OOH + H_2O).[7] Therefore, more eficient means of promoting •OH generation are necessary, such as using a

https://doi.org/10.1021/acs.nanolett.3c00696
Nano Lett. 2023, 23, 6323−6329

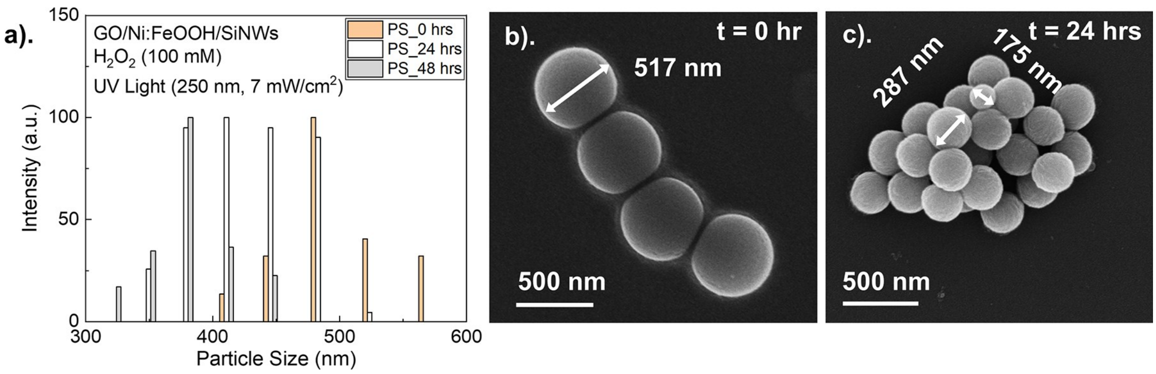

Figure 4. Degradation of 1 mg/L 500 nm diameter PS particles in 100 mM H_2O_2 for 24 and 48 h under 7 mW/cm^2 250 nm UV light. (a) Particle size distribution plot of PS samples before and after UV light irradiation. (b) SEM image of PS particles before UV irradiation. (c) SEM image of PS particles after UV irradiation for 24 h with GO/Ni:FeOOH/SiNWs.

photocatalyst that can produce large amounts of •OH at low H_2O_2 concentrations.

We further evaluated the performance of GO/Ni:FeOOH/SiNWs by measuring the degradation time dependence of 50 μM MB by 5 mM H_2O_2 via the following experiments: (1) no irradiation and no photocatalyst present, (2) UV irradiation without a photocatalyst, and (3) UV irradiation with GO/Ni:FeOOH/SiNWs. Figure 3d plots the normalized MB concentration (as its initial concentration) as a function of time. H_2O_2 itself barely degrades MB; the UV/H_2O_2 system reduced 50 μM MB dye to 24% after 60 min. GO/Ni:FeOOH/SiNWs exhibited considerably better performance as the level of the 50 μM MB dye was reduced to 1.5% after 60 min. These results strongly support the hypothesized improved •OH generation capability of GO/Ni:FeOOH/SiNWs in a UV/H_2O_2 system. In addition, the MB dye degradation eficiency of GO/Ni:FeOOH/SiNWs is higher than that of the previously reported best photocatalyst in the literature (SiNW/GO) demonstrated by Gaidi et al.[21] GO/Ni:FeOOH/SiNWs showed 98.5% 50 μM MB degradation after 30 min and 7 mW/cm^2 UV light illumination, while SiNW/GO showed 92% 20 μM MB degradation after 120 min and 450 W UV irradiation.[21]

As •OH is known to be capable of degrading plastics,[30] we tested the eficacy of UV/H_2O_2 with GO/Ni:FeOOH/SiNWs in degrading microplastic PS particles. The photodegradation of PS was performed using GO/Ni:FeOOH/SiNWs in 1 mg/L 500 nm PS in 100 mM H_2O_2 10 mL solutions for 24 and 48 h under 250 nm UV light (7 mW/cm^2) irradiation. The PS particle size was measured by dynamic light scattering (DLS, Nanobrook Omni, Brookhaven Instruments) before and after the degradation test. For the size measurement, the particles were dispersed in water and ultrasonicated for 30 min to reduce the extent of agglomeration. As shown in Figure 4a, the medium PS particle diameter is ∼500 nm before the test, ∼400 nm after irradiation for 24 h, and ∼380 nm after irradiation for 48 h, which corresponds to a reduction in volume by approximately half. Also, the SEM images (Figure 4b,c) show a reduction in the diameter of some of the PS particles to ∼200 nm after irradiation for 24 h. These results suggest that GO/Ni:FeOOH/SiNWs can be used for microplastic degradation in water treatment, especially given that GO/Ni:FeOOH/SiNWs are supported on Si wafers so they can be easily added and removed from the system, facilitating their reuse and recycling.

We investigated the mechanism of generation of •OH from GO/Ni:FeOOH/SiNWs using the methanol (MA) as a hole (h^+) scavenger and *p*-benzoquinone (BQ) as an $•O_2^-$ scavenger. The UV light irradiation (250 nm, 7 mW/cm^2) time was 30 min and the H_2O_2 concentration was 5 mM. We used a relatively low H_2O_2 concentration to better study the dependence of •OH generation on the active species scavenger concentration. Figure 5a shows that the concentration of

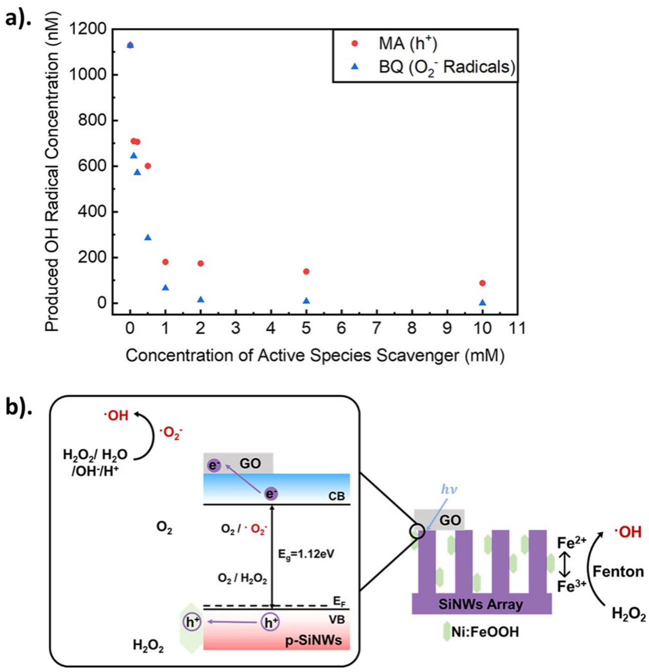

Figure 5. (a) •OH concentration produced as a function of scavenger concentration under 7 mW/cm^2 250 nm UV light irradiation for 30 min in 5 mM H_2O_2 of GO/Ni:FeOOH/SiNWs with 0–10 mM h^+ scavenger methanol (MA) and $•O_2^-$ scavenger *p*-benzoquinone (BQ). (b) Schematic of the reaction mechanism for the generation of •OH from GO/Ni:FeOOH/SiNWs.

produced •OH decreases with both increasing $•O_2^-$ scavenger BQ and increasing h^+ scavenger MA, indicating that both $•O_2^-$ and photogenerated h^+ concentration affect •OH generation.

Next, to better understand the photocatalytic mechanism involved in •OH generation, we photodeposited Ag (reacts with e^-) and CoOOH (reacts with h^+) particles to locate the spacial locations of the e^- and h^+ reactions. SiNWs produce e^-

https://doi.org/10.1021/acs.nanolett.3c00696
Nano Lett. 2023, 23, 6323−6329

and h^+ pairs by light absorption, followed by reduction of Ag^+ to Ag by e^- while Co^{2+} is oxidized to CoOOH by h^+ at the SiNW surface. Meanwhile, e^- and h^+ move along the SiNW in each direction. Therefore, the deposition of Ag and CoOOH identifies the direction of e^- and h^+ movement along the SiNW.

As shown in Figures S8 and S9, Ag is deposited mainly on GO while Co is deposited on the sidewalls of the SiNWs. This suggests that, in our GO/Ni:FeOOH/SiNWs system, the e^- transfers to GO while the h^+ transfers to the Ni:FeOOH flakes. We therefore propose the following •OH generation mechanism in our GO/Ni:FeOOH/SiNWs system as supported by the findings presented above (Figure 5b). Briefly, e^-/h^+ pairs are generated from the SiNWs by light absorption. In GO/Ni:FeOOH/SiNWs, when different materials are brought into contact with each other, their energy bands can align differently due to the difference in their work functions, and a built-in electrical field is formed. Such a built-in electric field facilitates the separation of electrons to GO and holes to Ni:FeOOH, which reduces the likelihood of recombination of the as-generated e^-/h^+ pairs. Electrons at the GO surface decrease the concentration of O_2 to form $•O_2^-$ (eq R5), while the holes at the Ni:FeOOH surface react with H_2O_2 to form $2h^+$ and O_2 (eq R6). The generated $•O_2^-$ can react with Fe^{2+} to form Fe^{3+} and H_2O_2 (eq R7), and $•O_2^-$ can react with water (H_2O), hydroxide ions (OH^-), or protons (h^+) to form additional •OH.[21,31,32] It should be noted that the generated $•O_2^-$ is also an effective oxidizer for organic dye degradation in addition to •OH.[31,32] Moreover, the Fe^{3+} in Ni:FeOOH enables the photo-Fenton reaction for the UV/H_2O_2 system (eqs R1–R4), promoting even more production of •OH. The use of Ni:FeOOH, compared to traditional Fenton reaction with Fe^{3+}, also removes the need to use acidic conditions.

$$e^- + O_2 \rightarrow •O_2^- \quad (R5)$$

$$2h^+ + H_2O_2 \rightarrow 2H^+ + O_2 \quad (R6)$$

$$Fe^{2+} + •O_2^- + 2H^+ \rightarrow Fe^{3+} + H_2O_2 \quad (R7)$$

In summary, we designed, fabricated, and demonstrated a multifunctional and effective GO/Ni:FeOOH/SiNW photocatalyst for producing •OH from H_2O_2 under UV irradiation, which increases the rate of generation of •OH in the UV/H_2O_2 system by 5.7 times and extends the light spectrum utilization to include visible light. We demonstrated that GO/Ni:FeOOH/SiNWs can degrade 98.5% MB dye after UV illumination for 60 min and that GO/Ni:FeOOH/SiNWs can reduce the size of 500 nm diameter PS particles by 20% after UV illumination for 24 h. Our mechanistic studies suggest that the built-in electrical field in GO/Ni:FeOOH/SiNWs facilitates the photogenerated e^- and h^+ in SiNWs to GO and Ni:FeOOH, respectively, with electrons then reducing the O_2 to form $•O_2^-$ while h^+ participates in further photochemical reactions in the system. The Ni:FeOOH also contributes to •OH formation through the photo-Fenton reaction. This work demonstrates the proof of concept of using GO/Ni:FeOOH/SiNWs to enhance the current H_2O_2 system for the advanced water oxidation process, but we note that further system engineering to optimize catalyst reusability (beyond 48 h as demonstrated in this work), to optimize the pH of the working medium, and to minimize the interference of coexisting ions and molecules that may be present in some water sources should be performed in the future. With continued efforts, GO/Ni:FeOOH/SiNWs could be implemented into more affordable and effective water purification systems to improve water sustainability and security in places where they are needed.

ASSOCIATED CONTENT

* Supporting Information

The Supporting Information is available free of charge at https://pubs.acs.org/doi/10.1021/acs.nanolett.3c00696.

Details of characterization of materials and testing methods and additional X-ray photoelectron spectroscopy, X-ray diffraction analysis, energy dispersive spectroscopy, and UV–visible spectroscopy data (PDF)

AUTHOR INFORMATION

Corresponding Author

Xiaolin Zheng – *Department of Mechanical Engineering, Stanford University, Stanford, California 94305, United States;* orcid.org/0000-0002-8889-7873; Email: xlzheng@stanford.edu

Authors

Rui Ning – *Department of Materials Science and Engineering, Stanford University, Stanford, California 94305, United States;* orcid.org/0000-0001-7719-9191

Sungsoon Kim – *Department of Mechanical Engineering, Stanford University, Stanford, California 94305, United States*

Eddie Sun – *Department of Mechanical Engineering, Stanford University, Stanford, California 94305, United States*

Yue Jiang – *Department of Mechanical Engineering, Stanford University, Stanford, California 94305, United States;* orcid.org/0000-0002-6017-8551

Jihyun Baek – *Department of Mechanical Engineering, Stanford University, Stanford, California 94305, United States;* orcid.org/0000-0002-1917-759X

Yuzhe Li – *Department of Mechanical Engineering, Stanford University, Stanford, California 94305, United States*

Ashley Robinson – *Department of Chemistry, Stanford University, Stanford, California 94305, United States;* orcid.org/0000-0002-2445-642X

Lauren Vallez – *Department of Mechanical Engineering, Stanford University, Stanford, California 94305, United States;* orcid.org/0000-0002-2605-0693

Complete contact information is available at: https://pubs.acs.org/10.1021/acs.nanolett.3c00696

Notes

The authors declare no competing financial interest.

ACKNOWLEDGMENTS

The authors acknowledge the support and funding provided by the California Energy Commission (CEC) for this research project. Part of this work was performed at the Stanford Nano Shared Facilities (SNSF), supported by the National Science Foundation under Grant ECCS-2026822. S.K. acknowledges the support from the International Energy Joint R&D Program of the Korea Institute of Energy Technology Evaluation and Planning (KETEP) and granted financial resources from the Ministry of Trade, Industry & Energy, Republic of Korea

(20208510010310). S.K. also acknowledges the support from BrainLink program funded by the Ministry of Science and ICT through the National Research Foundation of Korea (2022H1D3A3A01077254). E.S. acknowledges financial support from a National Science Foundation Graduate Research Fellowship under Grant DGE-165651 and by a Robert and Katherine Eustis Stanford Graduate Fellowship. X.Z. thanks the National Science Foundation EFRI-DCheM program (Agreement SUB0000425) for its generous support.

REFERENCES

(1) Deng, Y.; Zhao, R. Advanced oxidation processes (AOPs) in wastewater treatment. *Current Pollution Reports* 2015, *1*, 167−176.

(2) Liu, G.; Ji, J.; Huang, H.; Xie, R.; Feng, Q.; Shu, Y.; Zhan, Y.; Fang, R.; He, M.; Liu, S.; et al. UV/H2O2: An efficient aqueous advanced oxidation process for VOCs removal. *Chemical Engineering Journal* 2017, *324*, 44−50.

(3) Li, M.; Li, W.; Wen, D.; Bolton, J. R.; Blatchley, E. R., III; Qiang, Z. Micropollutant degradation by the UV/H2O2 process: kinetic comparison among various radiation sources. *Environ. Sci. Technol.* 2019, *53*, 5241−5248.

(4) Laera, G.; Cassano, D.; Lopez, A.; Pinto, A.; Pollice, A.; Ricco, G.; Mascolo, G. Removal of organics and degradation products from industrial wastewater by a membrane bioreactor integrated with ozone or UV/H2O2 treatment. *Environ. Sci. Technol.* 2012, *46*, 1010−1018.

(5) Pereira, V. J.; Weinberg, H. S.; Linden, K. G.; Singer, P. C. UV degradation kinetics and modeling of pharmaceutical compounds in laboratory grade and surface water via direct and indirect photolysis at 254 nm. *Environ. Sci. Technol.* 2007, *41*, 1682−1688.

(6) Zhao, Q.; Li, N.; Liao, C.; Tian, L.; An, J.; Wang, X. The UV/H2O2 process based on H2O2 in-situ generation for water disinfection. *Journal of Hazardous Materials Letters* 2021, *2*, 100020.

(7) Stasinakis, A. Use of selected advanced oxidation processes (AOPs) for wastewater treatment−a mini review. *Global NEST J.* 2008, *10*, 376−385.

(8) Ameta, R.; Chohadia, A. K.; Jain, A.; Punjabi, P. B. *Advanced oxidation processes for waste water treatment*; Elsevier, 2018; pp 49−87.

(9) Elmolla, E. S.; Chaudhuri, M. Photocatalytic degradation of amoxicillin, ampicillin and cloxacillin antibiotics in aqueous solution using UV/TiO2 and UV/H2O2/TiO2 photocatalysis. *Desalination* 2010, *252*, 46−52.

(10) García-Munoz, P.; Pliego, G.; Zazo, J.; Bahamonde, A.; Casas, J. Ilmenite (FeTiO3) as low cost catalyst for advanced oxidation processes. *Journal of Environmental Chemical Engineering* 2016, *4*, 542−548.

(11) Xu, M.; Wu, C.; Zhou, Y. In *Advanced Oxidation Processes*; Bustillo-Lecompte, C., Ed.; IntechOpen: Rijeka, Croatia, 2020; Chapter 4, pp 61−77.

(12) Cao, Y.; Shen, L.; Hu, X.; Du, Z.; Jiang, L. Low temperature desulfurization on Co-doped α-FeOOH: Tailoring the phase composition and creating the defects. *Chemical Engineering Journal* 2016, *306*, 124−130.

(13) Miao, X.; Dai, H.; Chen, J.; Zhu, J. The enhanced method of hydroxyl radical generation in the heterogeneous UV-Fenton system with α-FeOOH as catalyst. *Sep. Purif. Technol.* 2018, *200*, 36−43.

(14) da Silva Rocha, T.; Nascimento, E. S.; da Silva, A. C.; dos Santos Oliveira, H.; Garcia, E. M.; de Oliveira, L. C. A.; Monteiro, D. S.; Rodriguez, M.; Pereira, M. C. Enhanced photocatalytic hydrogen generation from water by Ni (OH) 2 loaded on Ni-doped δ-FeOOH nanoparticles obtained by one-step synthesis. *RSC Adv.* 2013, *3*, 20308−20314.

(15) Cai, L.; Zhao, J.; Li, H.; Park, J.; Cho, I. S.; Han, H. S.; Zheng, X. One-step hydrothermal deposition of Ni: FeOOH onto photoanodes for enhanced water oxidation. *ACS Energy Letters* 2016, *1*, 624−632.

(16) Saga, T. Advances in crystalline silicon solar cell technology for industrial mass production. *NPG Asia Materials* 2010, *2*, 96−102.

(17) Glunz, S. W. High-efficiency crystalline silicon solar cells. *Adv. OptoElectron.* 2007, *2007*, 97370.

(18) Qiu, X.; Yu, X.; Yuan, S.; Gao, Y.; Liu, X.; Xu, Y.; Yang, D. Trap assisted bulk silicon photodetector with high photoconductive gain, low noise, and fast response by Ag hyperdoping. *Advanced Optical Materials* 2018, *6*, 1700638.

(19) Feng, X.; Qi, X.; Li, J.; Yang, L.; Qiu, M.; Yin, J.; Lu, F.; Zhong, J. Preparation, structure and photo-catalytic performances of hybrid Bi2SiO5 modified Si nanowire arrays. *Appl. Surf. Sci.* 2011, *257*, 5571−5575.

(20) Shao, M.; Cheng, L.; Zhang, X.; Ma, D. D. D.; Lee, S.-t. Excellent photocatalysis of HF-treated silicon nanowires. *J. Am. Chem. Soc.* 2009, *131*, 17738−17739.

(21) Gaidi, M.; Daoudi, K.; Columbus, S.; Hajjaji, A.; El Khakani, M. A.; Bessais, B. Enhanced photocatalytic activities of silicon nanowires/graphene oxide nanocomposite: Effect of etching parameters. *J. Environ. Sci.* 2021, *101*, 123−134.

(22) Li, B.; Niu, G.; Sun, L.; Yao, L.; Wang, C.; Zhang, Y. Design optimization and antireflection of silicon nanowire arrays fabricated by Au-assisted chemical etching. *Materials Science in Semiconductor Processing* 2018, *82*, 1−8.

(23) Liang, J.; Li, Z.; Anang, E.; Liu, H.; Fan, X. Coupling Removal of P-Chloronitrobenzene and Its Reduction Products by Nano Iron Doped with Ni and FeOOH (nFe/Ni-FeOOH). *Materials* 2022, *15*, 1928.

(24) Weisse, J. M.; Lee, C. H.; Kim, D. R.; Cai, L.; Rao, P. M.; Zheng, X. Electroassisted transfer of vertical silicon wire arrays using a sacrificial porous silicon layer. *Nano Lett.* 2013, *13*, 4362−4368.

(25) Weisse, J. M.; Reifenberg, J. P.; Miller, L. M.; Scullin, M. L. Ultra-long silicon nanostructures, and methods of forming and transferring the same. U.S. Patent 9,691,849, 2017.

(26) Biesinger, M. C.; Payne, B. P.; Lau, L. W.; Gerson, A.; Smart, R. S. C. X-ray photoelectron spectroscopic chemical state quantification of mixed nickel metal, oxide and hydroxide systems. *Surf. Interface Anal.* 2009, *41*, 324−332.

(27) Grosvenor, A.; Kobe, B.; Biesinger, M. C.; McIntyre, N. Investigation of multiplet splitting of Fe 2p XPS spectra and bonding in iron compounds. *Surf. Interface Anal.* 2004, *36*, 1564−1574.

(28) Zhang, W.; Wu, Y.; Qi, J.; Chen, M.; Cao, R. A thin NiFe hydroxide film formed by stepwise electrodeposition strategy with significantly improved catalytic water oxidation efficiency. *Adv. Energy Mater.* 2017, *7*, 1602547.

(29) Wang, T.; Jiang, Z.; Chu, K. H.; Wu, D.; Wang, B.; Sun, H.; Yip, H. Y.; An, T.; Zhao, H.; Wong, P. K. X-shaped α-FeOOH with enhanced charge separation for visible-light-driven photocatalytic overall water splitting. *ChemSusChem* 2018, *11*, 1365−1373.

(30) Feng, H.-M.; Zheng, J.-C.; Lei, N.-Y.; Yu, L.; Kong, K. H.-K.; Yu, H.-Q.; Lau, T.-C.; Lam, M. H. Photoassisted Fenton degradation of polystyrene. *Environ. Sci. Technol.* 2011, *45*, 744−750.

(31) Gupta, N. K.; Ghaffari, Y.; Kim, S.; Bae, J.; Kim, K. S.; Saifuddin, M. Photocatalytic degradation of organic pollutants over MFe2O4 (M= Co, Ni, Cu, Zn) nanoparticles at neutral pH. *Sci. Rep.* 2020, *10*, 4942.

(32) Jia, J.; Guo, X.; Zhang, T.; Zha, F.; Tang, X.; Tian, H. Design of micro-nano spherical β-NiOOH/FeMoO4 composite with enhanced photo-Fenton performance. *Applied Catalysis A: General* 2022, *630*, 118427.